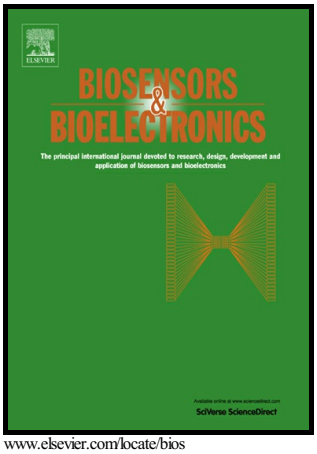

www.elsevier.com/locate/bios

A novel non-invasive detection method for the FGFR3 gene mutation in maternal plasma for a fetal Achondroplasia diagnosis based on signal amplification by hemin-MOFs/PtNPs

Jun Chen, Chao Yu, Yilin Zhao, Yazhen Niu, Lei Zhang, Yujie Yu, Jing Wu, Junlin He

PII: S0956-5663(16)31088-0
DOI: http://dx.doi.org/10.1016/j.bios.2016.10.067
Reference: BIOS9289

To appear in: *Biosensors and Bioelectronic*

Received date: 19 August 2016
Revised date: 12 October 2016
Accepted date: 25 October 2016

Cite this article as: Jun Chen, Chao Yu, Yilin Zhao, Yazhen Niu, Lei Zhang, Yujie Yu, Jing Wu and Junlin He, A novel non-invasive detection method for the FGFR3 gene mutation in maternal plasma for a fetal Achondroplasia diagnosi based on signal amplification by hemin-MOFs/PtNPs, *Biosensors an Bioelectronic,* http://dx.doi.org/10.1016/j.bios.2016.10.067

A novel non-invasive detection method for the FGFR3 gene mutation in maternal plasma for a fetal Achondroplasia diagnosis based on signal amplification by hemin-MOFs/PtNPs

Jun Chen[1], Chao Yu[1], Yilin Zhao, Yazhen Niu, Lei Zhang, Yujie Yu, Jing Wu, Junlin He*

School of Public Health，College of Pharmacy and Institute of Life Science, Chongqing Medical University, Chongqing 400016, P.R. China

*Corresponding author: Tel.: +(86) 23 68485378; fax: +(86) 23 68485161. hejunlin_11@aliyun.com

Full address: Box 197#, College of Pharmacy, Chongqing Medical University, No.1 ,Yi Xue Yuan Road, Yuzhong district，Chongqing 400016, P. R. China.

Abstract

The small amount of cell-free fetal DNA (cffDNA) can be a useful biomarker for early non-invasive prenatal diagnosis (NIPD) of achondroplasia. In this study, a novel non-invasive electrochemical DNA sensor for ultrasensitive detecting FGFR3 mutation gene, a pathogenic gene of achondroplasia, based on biocatalytic signal materials and the biotin-streptavidin system are presented. Notably encapsulation of hemin in metal-organic frameworks-based materials (hemin-MOFs) and platinum nanoparticles (PtNPs) were used to prepare hemin-MOFs/PtNPs composites via a one-beaker-one-step reduction. We utilized hemin-MOFs/PtNPs for signal amplification because the promising hemin-MOFs/PtNPs nanomaterial has remarkable ability of catalyze H_2O_2 as well as excellent conductivity. To further amplify the electrochemical signal, reduced graphene oxide-tetraethylene pentamine (rGO-TEPA), gold nanoparticles and streptavidin were selected for modification of the electrode to enhance the conductivity and immobilize more biotin-modified

[1] Chao Yu and Jun Chen contributed equally to this work.

capture probe (Bio-CP) through the high specificity and superior affinity between streptavidin and biotin. The electrochemical signal was primarily derived from the synergistic catalysis of H_2O_2 by hemin and PtNPs and recorded by Chronoamperometry. Under the optimal conditions, this newly designed biosensor exhibited sensitive detection of FGFR3 from 0.1fM to 1nM with a low detection limit of 0.033fM (S/N=3). We proposed that this ultrasensitive biosensor is useful for the early non-invasive prenatal diagnosis of achondroplasia.

Keywords: cffDNA; non-invasive electrochemical DNA sensor; hemin; MOF; biotin-streptavidin; synergistic catalytic

1. Introduction

Achondroplasia, the most common non-lethal skeletal dysplasia with a prevalence of 1/30,000 to 1/20,000 in live-born infants, is an inherited autosomal dominant disease and causes severe dwarfism (Hecht et al. 2014; Kara 2003; Zhao et al. 2015). More than 98% of patients with achondroplasia have a c.1138G>C mutation in the fibroblast growth factor receptor 3 gene (FGFR3) (Chitty et al. 2015; Kara 2003). Therefore, detection of the FGFR3 gene mutation allows for the early diagnosis of achondroplasia in pregnant women. According to the literature, electrophoretic separations, radioisotopic detection, restriction fragment length polymorphism assay and gene chip detection technologies are the traditional methods for FGFR3 gene mutation detection (Chitty et al. 2015; Horton et al. 2007; Kara 2003; Shiang et al. 1994). However, these methods have some limitations, such as labour-intensive, time-consuming, expensive and requiring complex instruments. In particular, conventional prenatal diagnosis requires the analysis of fetal material obtained following invasive procedures, such as chorionic villus sampling and amniocentesis (Tabor and Alfirevic 2010). Unfortunately, these invasive procedures exists significant procedural risks and cannot be offered to women who decline invasive methods (Xu et al. 2015). Thus, a non-invasive diagnosis method to detect FGFR3 gene mutation is urgent requirement.

Recently, the discovery that small amounts of cell-free fetal DNA (cffDNA)

circulate in the maternal bloodstream during pregnancy (Hall et al. 2010) presents a novel opportunity for the early non-invasive prenatal diagnosis (NIPD) based on the analysis of maternal blood (Lo et al. 1997). The detection of cffDNA in maternal plasma or serum may guide pregnancy management and aid reproductive decision-making (Hall et al. 2010). In recent years, using cffDNA to detect hereditary disease related genes for preventing birth defects has received great attention. Quantitative fluorescent PCR and whole-genome sequencing were used to analysis of cffDNAs for NIPD (Lo et al. 1998; Zhao et al. 2015). However, these technologies also have some deficits, such as being time-consuming, expensive and complex. Therefore, the development of an alternative method using cffDNA for early non-invasive prenatal testing of achondroplasia is critical for the clinical diagnosis of this disease.

Non-invasive electrochemical DNA sensors, in particular, have gained significant attention (Bandodkar and Wang 2014; Das et al. 2015; Drummond et al. 2003). Among the different types of non-invasive electrochemical DNA biosensors, “sandwich” type DNA sensors are used widely in clinical disease diagnosis because of the advantages of convenience, ultrasensitivity and selectivity. Herein, an ultrasensitive electrochemical DNA sensor was developed and is essential for detecting extremely low abundance DNA biomarkers in clinical samples. Frustratingly, the feasibility of analyzing cffDNAs for NIPD with electrochemical sensors has not been established. With this consideration, developing an ultrasensitive DNA sensor to detect a low concentration of FGFR3 gene mutations, specifically in the maternal bloodstream, has great significance for the NIPD of achondroplasia.

Hemin, a well-known natural metalloporphyrin, has peroxidase-like activity that is similar to the peroxidase enzyme (Guo et al. 2011; Xie et al. 2015) However, hemin as a catalyser often suffers from poor catalytic activity and stability in neutral and alkaline aqueous buffers (C.Bruice 1991). To overcome these problems, developing a matrix as a bracket for hemin to become a biomimetic catalyst with enhanced catalytic activity and stability is a promising method. Metal-organic frameworks (MOFs), due to their high specific surface areas, tunable pore sizes and exposed

active sites, are a new type of host matrix material to anchor hemin (Carne et al. 2011; Ma et al. 2013; Taylor-Pashow et al. 2009). Its excellent property could protect hemin as well as improve catalytic activity and catalytic life. Most studies only encapsulate hemin in MOF-based materials (hemin-MOFs) for the electrochemical or chemiluminescence detection of protein (or H_2O_2) (Luo et al. 2015; Xie et al. 2015). However, to the best of our knowledge, hemin-MOFs for the construction of a sandwich-type electrochemical DNA sensor were not developed.

Here, we report a novel enzyme-free electrochemical DNA sensor for the ultrasensitive detection of the FGFR3 mutation gene by encapsulating hemin into amino-contained Fe-MIL-88 MOFs and functionalized with platinum nanoparticles (PtNPs) as signal amplification tag. The Pt nanoparticle functionalized hemin-MOFs (hemin-MOFs/PtNPs) is able to load thiol modified signal probe (SP) through Pt-S bonds. For an immobilization biotinylated capture probe (Bio-CP) and further enhancing the sensitivity of our DNA sensor, we constructed a functional sensing interface by integrating reduced graphene oxide–tetraethylene pentamine (rGO-TEPA) with Au nanoparticles (AuNPs) and streptavidin. Deposit AuNPs on rGO-TEPA are able to enhance conductivity of our sensor due to the well conductivity of AuNPs and rGO-TEPA. Therefore, through amino-Au affinity, AuNPs can efficiently immobilize streptavdin. As we know, streptavidin with a large number of amino groups. The biotin-streptavidin system was selected due to the high specificity and strong affinity of streptavidin for biotin. Hemin-MOFs/PtNPs bioconjugates and biotin-streptavidin system have the following two major advantages: (1) compared to individual hemin-MOFs and PtNPs, our synthesized hemin-MOFs/PtNPs composites have the most efficient catalytic ability and are used as a signal amplification enhancer because of the syncatalytic changes of H_2O_2 by hemin-MOFs and PtNPs, (2) biotin-streptavidin system provides rich active sites for immobilization of the capture probes and also improves the sensitivity of the proposed non-invasive electrochemical DNA sensor. This proposed electrochemical DNA sensor showed ultrasenstivity, good stability, precision, and reproducibility, suggesting a wide range of potential diagnostic applications to detect low amounts of cffDNAs for NIPD.

2. Experimental

2.1. Materials and chemicals

Hemin, gold (III) chloride trihydrate ($HAuCl_4 \cdot 4H_2O$), chloroplatinic acid (H_2PtCl_6), streptavidin, Dimethylformamide (DMF) and 2-aminoterephthalic acid were obtained from Sigma-Aldrich (St. Louis, USA, www.sigmaaldrich.com). Reduced graphene oxide-tetraethylene pentamin (rGO-TEPA) was obtained from Nanjing XFNANO Materials TECH Co., Ltd. (China). Bovine serum albumin (BSA), potassium ferricyanide ($K_3Fe(CN)_6$) and potassium ferrocyanide ($K_4Fe(CN)_6$) were provided by Beijing Chemical Reagents Company (Beijing, China). $FeCl_3 \cdot 6H_2O$, H_2O_2, $NaBH_4$, and acetic acid and were purchased from Chongqing Chuandong Chemical Group Co., Ltd (Chongqing, China). Healthy pregnancy serums were obtained from the First Affiliated Hospital of Chongqing Medical University (Chongqing, China). DNA oligonucleotides were purchased from Sangon Biotech Co., Ltd. (Shanghai, China). Their sequences are provided in Table S1.

The buffer solutions involved in this study were as follow: 1 × TE buffer (10 mM Trishydroxymethylaminomethane hydrochloride (Tris-HCl), and 1.0 mM ethylenediaminetetraacetic acid (EDTA), pH 8.0), which was used to dissolve all oligonucleotides. The other buffer solutions are listed in Table S2. All other reagents were of analytical reagent grade and used without further purification. Ultrapure water (> 18.2 MΩ) obtained from a Millipore Mill-Q purification system was used throughout the experiment.

2.2. Apparatus and characterization

All electrochemical experiments were performed with a CHI660D electrochemical workstation (Chenhua Instruments Co., Shanghai, China). The images of different nanomaterials were characterized by scanning electron microscopy (SEM, S-4800, Hitachi, Tokyo, Japan) at an acceleration voltage of 5.0

kV. Field emission scanning electron microscopy (FE-SEM) image were obtained using a Hitachi S4800 (Hitachi Limited, Japan). X-ray photoelectron spectroscopy (XPS) was implemented using a VG Scientic ESCALAB 250 spectrometer (Thermoelectricity Instruments, USA) with an Al Ka X-ray (1486.6 eV) as the light source. Fourier transform infrared (FT-IR) spectroscopy was performed with a Nicolet 6700 FT-IR spectrometer (Thermo Nicolet, USA). Energy dispersive X-ray spectroscopy (EDS) was scaled using a JEOL JSM-6700F microscope (Japan). Atomic force microscopy (AFM) images were monitored by Bruker Dimension icon (USA). Agarose gel was photographed under UV light using a Quantum ST5 gel imaging system (Vilber, France). A conventional three-electrode system was used for all electrochemical measurements, consisting of a platinum wire electrode as the counter electrode, a saturated calomel electrode (SCE) as the reference electrode, and a modified glassy carbon electrode (GCE, 4 mm in diameter) as the working electrode.

2.3. Preparation of Fe-MIL-88 MOFs and hemin-MOFs/PtNPs

Fe-MIL-88 MOFs was synthesized as previously described (Liu et al. 2013). hemin-MOFs/PtNPs were prepared according to the literature with slight modifications (Xie et al. 2015). Briefly, 0.692 mM (0.187 g) of $FeCl_3$•$6H_2O$, 0.346 mM (0.226 g) of hemin, and 0.692 mM (0.126 g) of 2-aminoterephthalic acid were dissolved in 15 mL of DMF. The mixture solution was then placed in a silicone oil bath at 120 °C for 4 h, and 3.45 mM acetic acid was added to this solution after heating for 15 min. Following slow cooling to room temperature, the obtained hemin-MOFs were isolated by centrifugation and washed with DMF, ethanol and ultrapure water to remove surplus reactants. Finally, the precipitate was dried in a vacuum oven overnight. Hemin-MOFs/PtNPs were synthesized using the $NaBH_4$ reduction method. First, 1 mL of H_2PtCl_6 (1%) was added to 1 mL of a prepared hemin-MOFs solution (1 mg mL^{-1}) and vigorously sonicated for 20 min. Subsequently, 2 mL of a $NaBH_4$ (0.1 M) solution was added dropwise into the mixture with stirring

for 30 min at 400 rpm. Then, the mixture was isolated by centrifugation and washed with ultrapure water three times. Accordingly, the PtNPs were assembled on the surface of hemin-MOFs *via* Pt-S bonds to enhance the electrical conductivity of hemin-MOFs and immobilize SP in the next step.

2.4. Preparation of the hemin-MOFs/PtNPs-SP-BSA, hemin-MOFs/AuNPs-SP-BSA, MOFs/AuNPs-SP-BSA, and MOFs/PtNPs-SP-BSA

The detailed procedure for synthesizing the MOFs/AuNPs, MOFs/PtNPs and hemin-MOFs/AuNPs nanocomposite were provided in the Supplementary Information (S1). In brief, 200 μL of thiol-terminated SP (2 μM) was added to 2 mL of a prepared hemin-MOFs/PtNP solution and stirred for 12 h at 4 °C. Subsequently, BSA was added to the above mixture for 4 h to block non-specific binding sites on the surface of hemin-MOFs/PtNPs. Then, hemin-MOFs/PtNPs-SP-BSA bioconjugates were centrifuged at 8 000 rpm for 5 min and washed three times with ultrapure water. Prior to use, the bioconjugates were dispersed in 2 mL of hybridization buffer (pH 7.4) and stored at 4 °C. The hemin-MOFs/AuNPs-SP-BSA, MOFs/AuNPs-SP-BSA and MOFs/PtNPs-SP-BSA bioconjugates were synthesized using a similar process for hemin-MOFs/PtNPs-SP-BSA, except that hemin-MOFs/PtNPs were displaced by hemin-MOFs/Au-NPs, MOFs/AuNPs and MOFs/PtNPs, respectively.

2.5. Construction of the Electrochemical DNA Biosensor

The fabrication procedure of the electrochemical DNA biosensor is outlined in Scheme 1. To achieve a mirror-like surface, GCE was polished repeatedly with 0.3 and 0.05 μm alumina slurries followed by a thorough rinsing with ultrapure water. After washing ultrasonically in baths of ultrapure water, absolute alcohol and ultrapure water, successively, the electrode was dried at room temperature. Then, 6 μL of rGO-TEPA aqueous suspension (2 mg mL^{-1}) was cast onto the electrode surface and air-dried. Subsequently, to obtain a larger conductive surface area and more active sites for the immobilized streptavidin, AuNPs were electrochemically deposited onto the rGO-TEPA-modified GCE surface under a constant potential of –0.2 V for 30 s in

a 1% $HAuCl_4$ solution. After washing with ultrapure water, 10 μL of the streptavidin solution (1 μg mL^{-1}) was dropped onto the modified electrode surface and streptavidin combined with AuNPs via Au-NH_2 bonded. The electrode was placed at 4 °C overnight to allow the streptavidin to more efficiently bond with the Au nanoparticles. After the reaction, the electrode was washed with ultrapure water to remove loosely bound reactants and then dried in nitrogen. Next, 10 μL of Bio-CP (1 μM) was added onto the as-prepared electrode surface for 12 h at 4 °C, resulting in the immobilization of Bio-CP on the modified electrode through streptavidin-biotin affinity. After that, the electrode was rinsed with ultrapure water and blocked with a BSA solution (0.25%, w/v) for 30 min at room temperature to eliminate nonspecific binding sites between the analyte and electrode. In order to fabricate the sandwiched modality, first, the as-prepared electrodes were incubated with various concentrations of target DNA in DNA hybridization buffer (pH 7.4) for 2 h at 37 °C. Next, 10 μL of the prepared hemin-MOFs/PtNPs-SP-BSA bioconjugates was cast onto the electrode surface and incubated for an additional 2 h. Subsequently, the electrodes were rinsed with ultrapure water and prepared for electrochemical measurement.

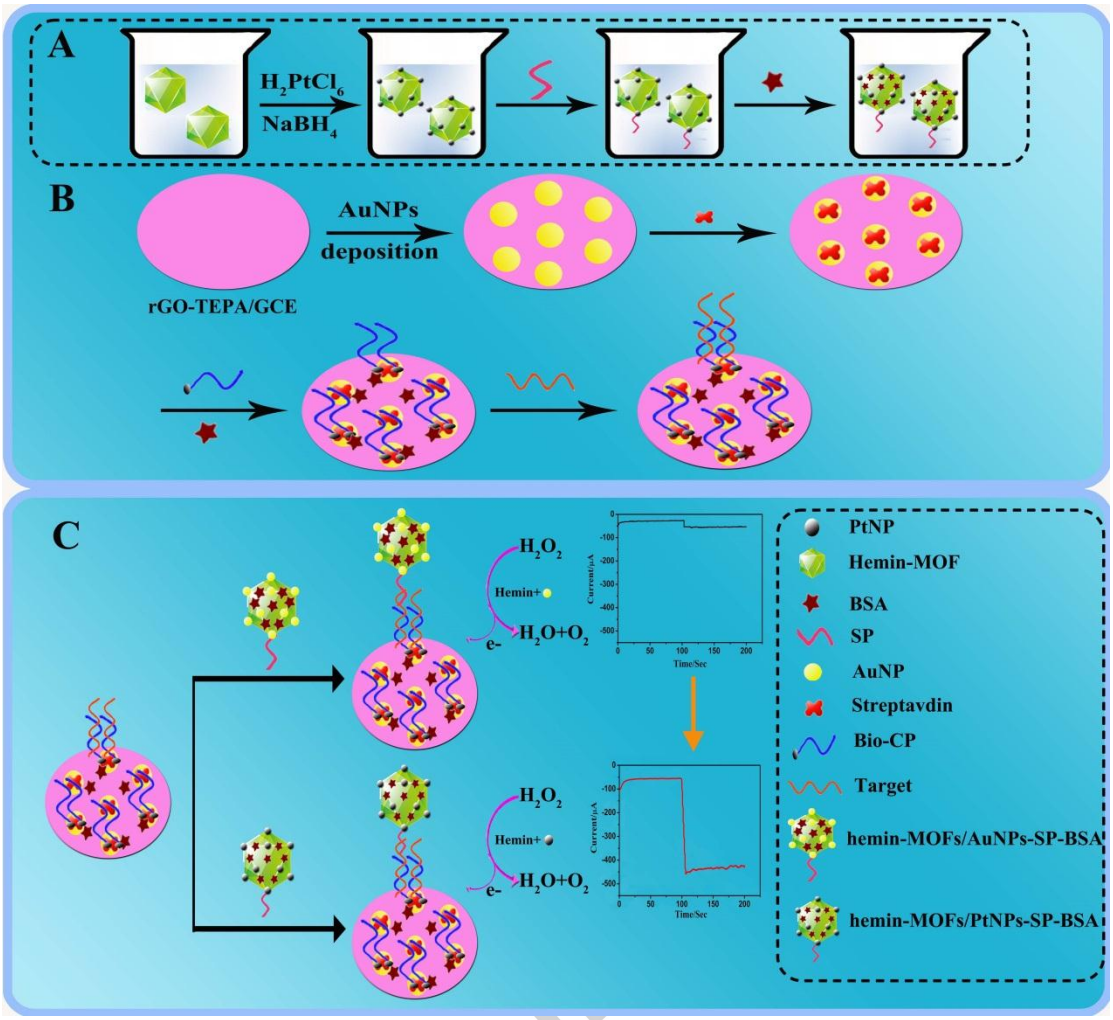

Scheme 1. (A) The preparation of hemin-MOFs/PtNPs-SP-BSA bioconjugates. (B) Schematic illustration of the stepwise assembly procedure of the electrochemical DNA sensor interface. (C) Schematic representation of the electrochemical DNA sensor and signal amplification mechanism.

2.6. Measurement procedure

Based on the typical procedure for the sandwich-type DNA assay, 10 μL of the as-prepared hemin-MOFs/PtNPs-SP-BSA bioconjugates were added onto the electrodes followed by incubation for 2 h at 37 °C.

To perform the electrochemical measurement, the amperometric i-t curves were recorded at -0.4 V in 5 mL of working buffer (pH 7.4) at room temperature. After the background current was stable, 20 μL of H_2O_2 (1.2 mmol L^{-1}) was added to the solution and the current changes were recorded.

3. Results and discussion

3.1. Characterization of different nanomaterials

SEM and FE-SEM were used to elucidate the size and morphology of the as-prepared nanomaterials. As shown in Fig. 1A, most of the Fe-MIL-88 MOFs showed a regular octahedron structure with an average diameter of approximately 100 nm, which was consistent with the previous report (Liu et al. 2013). However, the synthesized hemin-MOFs presented some different octahedron morphologies from the FE-SEM image (Fig. 1B), indicating that the encapsulation of hemin in Fe-MIL-88 MOFs affected the morphology of MOFs. After the hemin-MOFs was functionalized with PtNPs, distinguish from pure hemin-MOFs, a large amount of bright dots spread along the hemin-MOFs were observed, as shown in Fig. 1C.

To further confirmed the successful synthesis of hemin-MOFs/PtNP composites, EDS and XPS were used for elemental analysis. As shown in Fig. 1D, there are significant peaks corresponding to C, N, O, Pt and Fe in the EDS image. Furthermore, the characteristic peaks for the Pt4f, C1s, N1s, O1s and Fe2p core level regions are clearly observed in the hemin-MOFs/PtNPs composites from the XPS image. The composites showed the spectrum of C1s, N1s, O1s and Fe2p, indicating the successful synthesis of amino-contained hemin-MOFs. Moreover, the Pt4f core level suggested that the hemin-MOFs/PtNPs effectively anchored PtNPs. The spectrum of Fe2p and Pt4f are displayed in Fig. 1F and Fig. 1G. These results reveal that hemin-MOFs/PtNP composites were successfully synthesized. A further demonstration of the formation of the hemin-MOFs composites by cyclic voltammetry (CV) and FT-IR are displayed in Fig. S1.

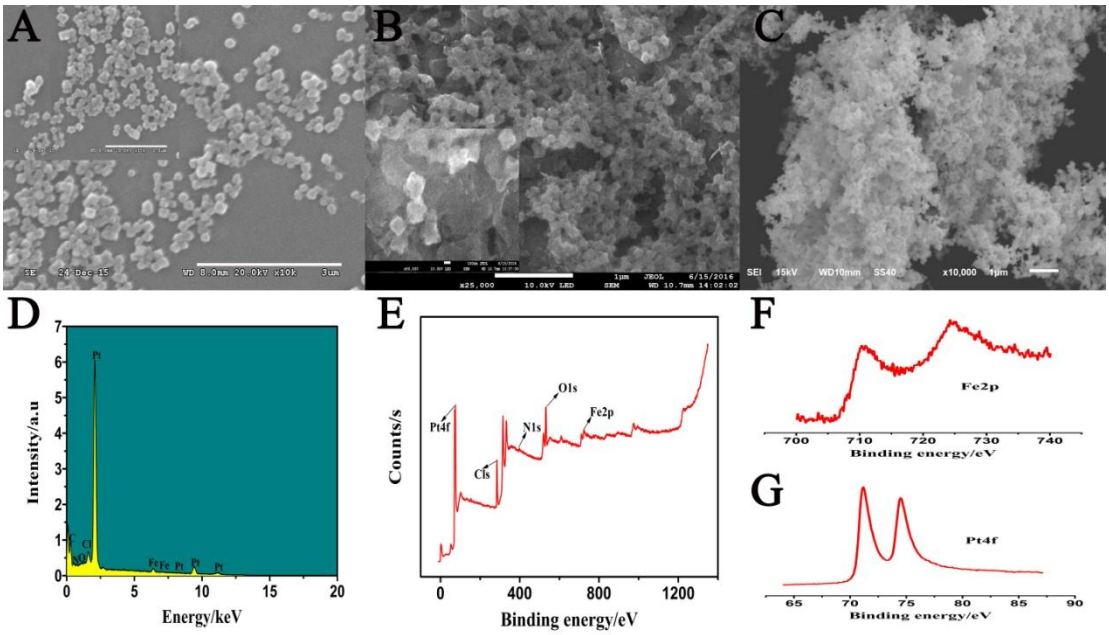

Fig. 1. SEM image of Fe-MIL-88 MOFs (A), and FE-SEM image of hemin-MOFs (B). SEM image of hemin-MOFs/PtNPs (C). EDS of hemin-MOFs/PtNPs (D). The XPS spectrum of hemin-MOFs/PtNPs (E). The spectra of Fe2p in hemin-MOFs/PtNPs (F) and Pt4f in hemin-MOFs/PtNPs (G).

3.2. Agarose gel electrophoresis analysis

Successful coupling among the target DNA, bio-CP and SP was investigated by agarose gel electrophoresis in Fig. S2. The analysis by electrophoresis was performed with 5% agarose gel electrophoresis run in 0.5×TBE buffer (pH 7.9) at room temperature, followed by nucleic acid dye staining. Subsequently, loading 8 uL of each prepared sample into the lanes, the electrophoresis experiments were performed at a 90 V constant voltage for 0.5 h.

3.3. Characteristics of modified electrodes

The stepwise DNA biosensor fabrication procedure was assessed using SEM, and the results are shown in detail in the Supplementary Information (Fig. S3).

3.4. Electrochemical characterization of the stepwise modified electrodes

CV and electrochemical impedance spectroscopy (EIS) measurements were performed step by step in a 5 mM $[Fe(CN)_6]^{3-/4-}$ solution. The CV measurements were

executed within a scan rate of 50 mV s^{-1} and a voltage range of −0.3 V to 0.7 V. The EIS parameters was carried out included a 5 mV amplitude and frequency range of 1×10^{-3}–1×10^{-5} Hz at room temperature. As shown in Fig. 2A, a pair of typical reversible redox peaks are observed, corresponding to the reversible redox reaction of $[Fe(CN)_6]^{3-/4-}$ on bare GCE (curve a). After the rGO-TEPA was coated onto the electrode, the peak current of CV increased (curve b) because of the excellent electrical conductivity of rGO-TEPA. When AuNPs were electrodeposited on the rGO-TEPA/GCE, the peak current signally increased (curve c) because the conductively AuNPs could accelerated the electron transfer. After the modified electrode was combined with streptavidin, a marked decrease in peak current was observed (curve d) because of the poor conductivity of streptavidin. When the Bio-CP was assembled onto the streptavidin surface, the peak current was further decreased because of the electrostatic repulsion between the negative charges of the capture probe phosphate backbone and the $[Fe(CN)_6]^{3-/4-}$ ions (curve e). Non-conductive BSA as blocking agent caused the peak current to decrease again (curve f). Moreover, the peak current further decreased after incubation with the target (curve g) because target can hybridize with Bio-CP and more negatively charged DNA strands were loaded onto the electrode surface. Meanwhile, we also used CV to analyze element characteristic peak for characterize the assembly process of DNA sensor in a 0.5 M H_2SO_4 solution and shown in Supplementary information (Fig. S4).

EIS was used to further validate the stepwise-modified processes of the proposed electrode in a 5 mM $[Fe(CN)_6]^{3-/4-}$ solution. In the Nyquist diagram, the semicircle diameter is equivalent to the electron transfer resistance, and the linear part of the curve at low frequency represents the diffusion process. As shown in Fig. 2B, when rGO-TEPA was coated onto the electrode, the resistance decreased (curve b) compared to the bare GCE (curve a) because rGO-TEPA can accelerate the electron transfer of the electrode. After AuNPs were electrodeposited onto the electrode, the diameter of the semicircle was decreased (curve c), indicating that AuNPs accelerated electron transfer between the electrode and the solution. When streptavidin was dropped onto the electrode, the resistance was increased (curve d), suggesting that

non-conductive streptavidin was successively immobilized onto the electrode. The resistance increased significantly (curve e) after the electrode was incubated with the Bio-CP, due to the electrostatic repulsion between the negative charges of the capture probe phosphate backbone and the $[Fe(CN)_6]^{3-/4-}$ ions. Afterwards, a large semicircle diameter was observed when the electrode was blocked with BSA (curve f) because BSA hindered electron transfer. Subsequently, with incubation of the target onto the electrode, the resistance was further increased (curve g), because more negative charges of phosphate backbone was obtained. At the same time, AFM is a useful approach to characterize the fabrication of the electrode. A detailed description can be found in the Supplementary Information (Fig. S5). All of these results obtained seem to further supported the successful fabrication of the proposed biosensor.

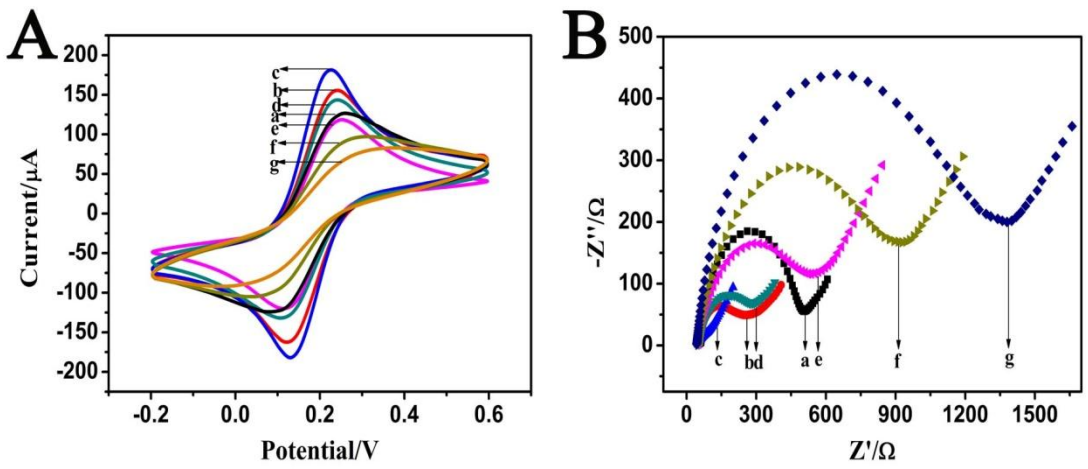

Fig. 2. (A) CV characterization of electrodes at various steps of modification in a 5 mM $[Fe(CN)_6]^{3-/4-}$ solution: (a) bare GCE, (b) rGO-TEPA/GCE, (c) AuNPs/rGO-TEPA/GCE, (d) streptavdin/AuNPs/rGO-TEPA/GCE, (e) Bio-CP/streptavdin/AuNPs/rGO-TEPA/GCE, (f) BSA/Bio-CP/streptavdin/AuNPs/rGO-TEPA/GCE, and (g) Target/BSA/Bio-CP/streptavdin/AuNPs/rGO-TEPA/GCE. (B) EIS for each immobilization step in 5 mM $[Fe(CN)_6]^{3-/4-}$: (a) bare GCE, (b) rGO-TEPA/GCE, (c) AuNPs/rGO-TEPA/GCE, (d) streptavidin/AuNPs/rGO-TEPA/GCE, (e) Bio-CP/streptavidin/AuNPs/rGO-TEPA/GCE, (f) BSA/Bio-CP/streptavidin/AuNPs/rGO-TEPA/GCE, and (g) Target/BSA/Bio-CP/streptavdin/AuNPs/rGO-TEPA/GCE.

3.5. Comparison of different signal amplification strategies

To validate the signal amplification strategies of the proposed protocol, the electrochemical DNA sensor was modified by different signal amplification tags (Fig.

3). All of the assay procedures were implemented with the same concentration of target DNA (100 pM). As shown in Fig. 3A, compared to the DNA sensor incubated with MOFs/AuNPs-SP-BSA, the DNA sensor incubated with hemin-MOFs/AuNPs-SP-BSA showed a clear increase in the electrochemical signal because both hemin and AuNPs could catalyses H_2O_2. Additionally, the electrochemical signal increased when the DNA sensor was incubated with MOFs/PtNPs-SP-BSA compared to the MOFs/AuNPs-SP-BSA (Fig. 3B) owing to the fact that the catalytic ability of PtNP is stronger than AuNP (Liu et al. 2014). Notably, the current increased more (curve b) in Fig. 3C when compared with the current increased (curve b) in Fig. 3A. This interesting phenomenon indicated that the DNA sensor were incubated with hemin-MOFs/PtNPs-SP-BSA have the most efficient catalytic ability, the probable reason was that the cooperative catalytic ability of PtNPs and hemin. As shown in Fig. 3D, the current was significantly increased when the DNA sensor was combined with the biotin-streptavidin system rather than simply used AuNPs. Owing to the fact that one streptavidin molecule can bind up to four biotin molecules and have the highest known affinity in nature (Li et al. 2016; Livnah et al. 1993). The comparison of the all results demonstrates that our proposed electrochemical DNA sensor could significantly improves the detection sensitivity.

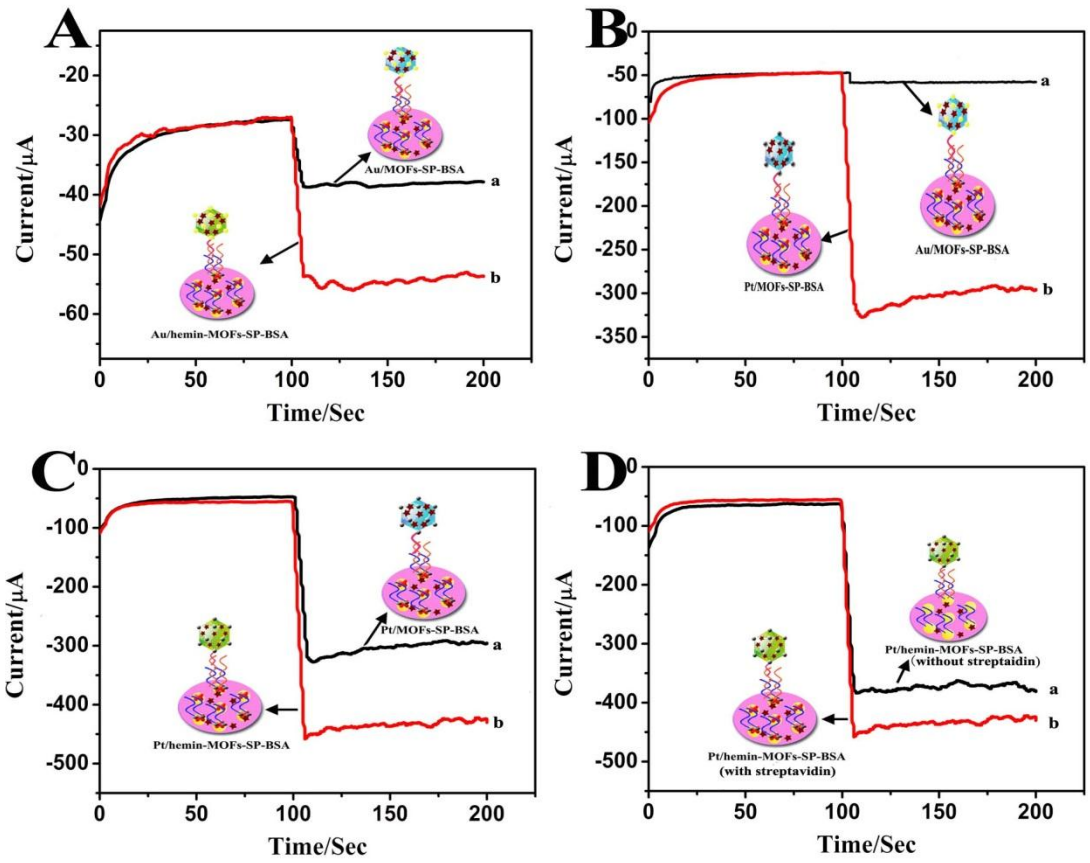

Fig. 3. The i-t curve of the as-prepared DNA sensor incubated with different composite material: (A) MOFs/AuNPs-SP-BSA (a) and hemin-MOFs/AuNPs-SP-BSA (b); (B) MOFs/AuNPs-SP-BSA (a) and MOFs/PtNPs-SP-BSA (b); (C) MOFs/PtNPs-SP-BSA (a) and hemin-MOFs/PtNPs-SP-BSA (b); and (D) hemin-MOFs/PtNPs-SP-BSA (without streptavdin, a) and hemin-MOFs/PtNPs-SP-BSA (with streptavidin, b).

3.6. Optimization of experimental conditions

To enhance the catalytic efficiency and obtain a high sensitivity of the proposed non-invasive electrochemical DNA sensor, it is necessary to optimize some crucial parameters, such as the concentration of rGO-TEPA, effects of the deposition time of AuNPs, concentration of streptavidin, immobilization time of the capture probe, hybridization time between the capture probe and target DNA, and concentration of H_2O_2. The quantity of PtNPs was displayed in the Supplementary Information. As shown in Fig. S6A, the current change increased rapidly with increasing the concentration of rGO-TEPA from 1.0 mg mL^{-1} to 2.0 mg mL^{-1} and then began to level off. The maximum current change appeared at 2.0 mg mL^{-1}. Therefore, 2.0 mg mL^{-1} was selected as the optimal concentration of rGO-TEPA for electrode modification.

Additionally, the AuNPs electro-deposition time is a critical factor for the layer thickness and quantity of AuNPs deposited. This time also plays a key role in providing a beneficial surface for streptavidin immobilization. As shown in Fig. S6B, the current change increased with the increasing deposition time of AuNPs from 10 s to 30 s. Subsequently, the current was gradually decreased after 30s. This phenomenon indicated that the excessive amount of AuNPs decreased the surface area of the electrode and hindered electron transfer (Gao et al. 2014). As a result, the electrode achieved the highest current change at a deposition time of 30 s. Therefore, the optimal deposition time of the AuNPs was 30 s.

The concentration of streptavidin is also an important factor for the Bio-CP immobilization and influencing biosensor performance. The concentration of streptavidin was tested in the range of 0.6-1.4 μg mL^{-1}. Fig. S6C shows that with an increased concentration of streptavidin, the current change first increased and then subsequently maintained a steady state. The maximum current change appeared at 1 μg mL^{-1}, suggesting that the amount of steptavidin on the surface of the sensor reaches a maximum based on the amino-Au affinity between AuNPs and streptavidin.Therefore, 1 μg mL^{-1} was selected as the optimal concentration of streptavidin.

For recognition of target DNA, the immobilization time of the Bio-CP is a remarkably important parameter. Therefore, the immobilization time of Bio-CP was investigated and is shown in Fig. S6D. Accompanying the increase of the immobilization time, the current change first increased quickly and remained steady at approximately 12 h, which was attributed to the saturation of biotin-streptavidin binding, indicating that the maximum immobilization of Bio-CP was obtained. To effectively hybridize target DNA in the following step, 12 h was selected as the optimal immobilization time.

The hybridization time is another important factor influencing the DNA biosensor response. As shown in Fig. S6E, the current change increased rapidly with an increase in hybridization time from 60 to 120 min and then levelled off after 120 min, indicating that the Bio-CP was completely hybridized to the target DNA. Therefore,

120 min was selected as the optimal hybridization time.

Furthermore, to achieve an optimal electrochemical signal, the concentration of H_2O_2 was investigated and is shown in Fig. S6F. The current change increased with an increase of H_2O_2 and then reached saturation after the addition of 1.2 mmol L^{-1} H_2O_2, demonstrating the highest efficiency of bioelectrocatalysis at this point. Therefore, 1.2 mmol L^{-1} of H_2O_2 was selected throughout the detection process.

The quantity of PtNPs is also a considerable factor influencing the catalytic efficacy of DNA biosensor. Thus, the quantity of PtNPs was investigated and is shown in Fig. S7. The current change significantly increased with an increase of the quantity of PtNPs and then remained steady at used 1% of H_2PtCl_6, indicating that the quantity of PtNPs in the surface of hemin-MOFs has reached the saturated state. Therefore, 1% of H_2PtCl_6 was selected throughout the detection process.

3.7. Analytical Performance of the electrochemical DNA biosensor

To evaluate the sensitivity and quantitative range of the proposed non-invasive electrochemical DNA sensor, the DNA sensors were incubated with different concentrations of target DNA under optimal conditions, and the amperometric i–t curve was recorded by adding 20 μL of H_2O_2 to the characterization solution every 100 s. As shown in Fig. 5A, the electrochemical signal gradually increased with increasing concentrations of target DNA in 5 mL of PBS (0.1 M, pH 7.4). The calibration plots showed a strong linear dependence of current on the logarithm of the target DNA concentration in the range from 0.1 fM to 1 nM, with a detection limit of 0.033 fM (based on S/N=3), and the results are shown in Fig. 5B. The regression equation was $Y=24.14*\log C_{target}+293.53$, with a correlation coefficient of 0.9992. The results indicated that the proposed electrochemical DNA sensor could be used to detect target DNA quantitatively. Furthermore, the performance comparison of the proposed DNA sensor with the other methods for FGFR3 gene mutation determination also performed. As shown in Table 1, The detection limit of this work for FGFR3 gene mutation determination seems to show few advantages than Kara et al(), however, they have used PCR to achieve signal amplification. Compared with

their method, our method was rapid and simple operation. We also have made a comparison of PtNPs and hemin in the biosensor between our study and other works (Table S2). The detection limit and linear ranges are superior to other methods. Therefore, we conclude that our proposed sensor exhibits a higher sensitivity. The detection limits of the proposed DNA biosensor can be used to detect FGFR3 gene mutation in practical use. Furthermore, our proposed method provides a foundation for the use of NIPD to detect other diseases.

3.8. Specificity, Stability and Reproducibility of the DNA biosensor

To determine whether the DNA sensor could accurately detect a point mutation, we challenged the DNA sensor with other oligonucleotides, such as single-base mismatch (mismatch-1), double-base mismatch (mismatch-2), three-base mismatch (mismatch-3) and non-complementary target (random). The current responses to each type of oligonucleotide were recorded in Fig. 5D. Even when 10-fold higher concentrations of oligonucleotides compared to target DNA were used, there were no obvious changes in current response in contrast to the blank assay. However, a marked increase was obtained in the presence of target DNA. The results indicate the high selectivity of the proposed DNA sensor.

To evaluate the stability of the DNA sensor, we investigated long-term storage. The DNA sensor was stored at 4 °C before use. There were no obvious changes during the first 3 days of storage, and the current changed were less than 1.5%. After 28 days of storage, it retained 94.5% of its initial current response (Fig. S8), which indicated that the proposed DNA sensor had good stability. The reproducibility of the DNA sensor was recorded by the assessment of the same concentration of target DNA (100 pM) using intra-assays and inter-assays (Fig. 5C). The RSD of the intra- and inter-assays were 2.76% and 2.58%, respectively. The results indicate that the proposed DNA sensor has acceptable reproducibility.

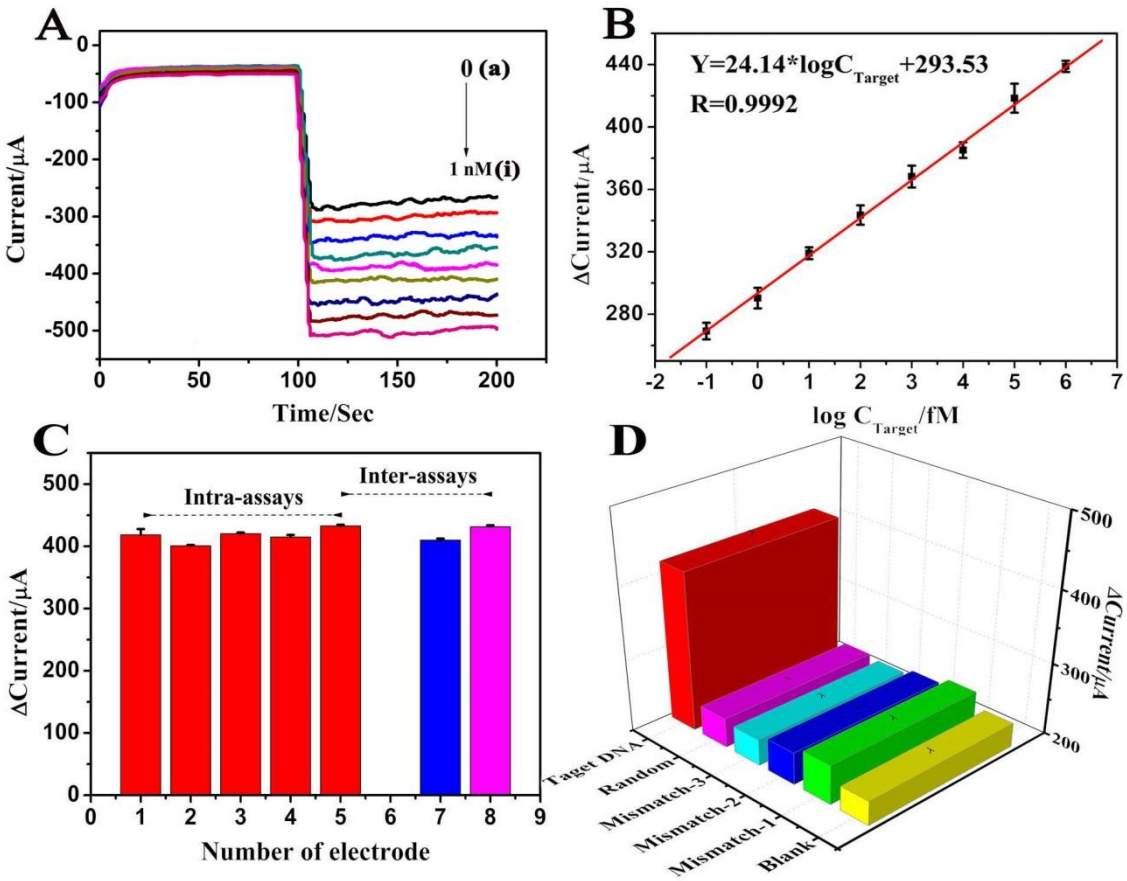

Fig. 5. (A) The i-t curve signals of the DNA sensor for the determination of different concentration of FGFR3: (a) 0 fM, (b) 0.1fM, (c) 1fM, (d) 10fM, (e) 100fM, (f) 1pM, (g) 10pM, (h) 100pM, and (i) 1nM. (B) The calibration curve of the DNA biosensor for different concentrations of FGFR3 (n = 3). (C) Reproducibility of 7 different electrodes modified with 100 pM of FGFR3. (D) Specificity of the DNA sensor towards the: zero analyte, 1nM mismatch-1, 1nM mismatch-2, 1nM mismatch-3, 1nM random, and 100pM target DNA

Table 1. Analytical performance compared with to other methods of FGFR3 gene mutation detection.

Sensor formats	Detection methods	Detection limit	Linear range	Reference
Label-free DNA sensor	Resonance wavelength	400 fM	400 fM to 3.2 pM	(Shin et al. 2013)
Electrochemical DNA chip	DPV	0.045 fM	-	(Kara 2003)
Non-invasive electrochemical DNA sensor	i-t	0.033 fM	0.1 fM to 1 nM	this study

3.9. Application for the analysis of serum samples

The fundamental purpose for developing a mutation-identifying non-invasive electrochemical DNA sensor is to enable the direct analysis of mutated sequences in patient samples. Some researchers proposed that the amount of cffDNAs increased with the increase in gestation time (Honda et al. 2002; Ingargiola et al. 2003). Here, to investigate the reliability of the proposed DNA sensor to detect different concentrations of FGFR3 in the maternal serum at different periods of gestation, recovery experiments were performed by adding different concentrations of target DNA to 10-fold diluted healthy pregnancy serum (obtained from the First Affiliated Hospital of Chongqing medical university, China). As shown in Table S4, the recovery and RSD ranged from 97.4% to 105.2% and from 3.26% to 4.12%, respectively, which demonstrated that the proposed DNA sensor can identify the FGFR3 gene mutation in different gestation periods from the actual maternal bloodstream.

4. Conclusion

In summary, we present an enzyme-free cooperative catalysis signal amplification approach for the ultrasensitive electronic detection of the FGFR3 gene mutation based on a novel non-invasive electrochemical DNA sensor. On the one hand, hemin-MOFs/PtNPs composites were first successfully synthesized and exhibited excellent electrocatalytic activity because of the cooperatively catalytic ability of PtNPs and hemin-MOFs. On the other hand, to enhance the sensitivity of the proposed DNA sensor, a biotin-streptavidin system was used. With these advantages, the biosensor showed a low detection limit and satisfied the sensitivity for low amounts of FGFR3 detection, demonstrating a new method for the determination of cffDNAs in clinical early non-invasive prenatal diagnosis applications. However, the proposed DNA sensor only tests for single-gene disorders, which may limit its use for detecting a polygenic disorder. Therefore, it is necessary to combine this approach

with other technologies, such as gene chip and micro-array technology, for its application in detecting polygenic disorder.

Acknowledgements

We are grateful for the financial support from the National Nature Science Foundation of China (No. 81370403), Chongqing foundation and advanced research project (No. CSTC2015jcyjBX0053), and Chongqing medical university scientific research cultivating fund(No.201414).

Reference

Bandodkar, A.J., Wang, J., 2014. Trends Biotechnol 32, 363-371.

C.Bruice, T., 1991. Accounts. Chem. Res. 24, 243-249.

Carne, A., Carbonell, C., Imaz, I., Maspoch, D., 2011. Chem. Soc. Rev. 40, 291-305.

Chitty, L.S., Mason, S., Barrett, A.N., McKay, F., Lench, N., Daley, R., Jenkins, L.A., 2015. Prenatal. Diag. 35, 656-662.

Das, J., Ivanov, I., Montermini, L., Rak, J., Sargent, E.H., Kelley, S.O., 2015. Nat. Chem. 7, 569-575.

Drummond, T.G., Hill, M.G., Barton, J.K., 2003. Nat. Biotechnol. 21, 1192-1199.

Gao, L., He, J., Xu, W., Zhang, J., Hui, J., Guo, Y., Li, W., Yu, C., 2014. Biosens. Bioelectron. 62, 79-83.

Guo, Y., Deng, L., Li, J., Guo, S., Wang, E., Dong, S., 2011. ACS. Nano. 5, 1282-1290.

Hall, A., Bostanci, A., Wright, C.F., 2010. Public. Health. Geno. 13, 246-255.

Hecht, J.T., Bodensteiner, J.B., Butler, I.J., 2014. Handb. Clin. Neurol. 119, 551-563.

Honda, H., Miharu, N., Ohashi, Y., Samura, O., Kinutani, M., Hara, T., Ohama, K., 2002. Hum. Genet. 110, 75-79.

Horton, W.A., Hall, J.G., Hecht, J.T., 2007. Lancet. 370, 162-172.

Ingargiola, I., Vaerman, J.L., Debieve, F., Palgen, G., Verellen-Dumoulin, C., Hubinont, C., 2003. Prenat. Diagn. 23, 1077-1082.

Kara, P., 2003. Clin. Chim. Acta. 336, 57-64.

Li, Q., Yu, C., Gao, R., Xia, C., Yuan, G., Li, Y., Zhao, Y., Chen, Q., He, J., 2016. Biosens. Bioelectron. 80, 674-681.

Liu, N., Wang, Z., Ma, Z., 2014. Bioanalysis. 6, 903-905.

Liu, Y.L., Zhao, X.J., Yang, X.X., Li, Y.F., 2013. Analyst. 138, 4526-4531.

Livnah, O., Bayer, E.A., Wilchek, M., Sussman, J.L., 1993. Proc. Natl. Acad. Sci. USA. 90, 5076-5080.

Lo, Y.M., Corbetta, N., Chamberlain, P.F., Rai, V., Sargent, I.L., Redman, C.W., Wainscoat, J.S., 1997. Lancet. 350, 485-487.

Lo, Y.M., Tein, M.S., Lau, T.K., Haines, C.J., Leung, T.N., Poon, P.M., Wainscoat, J.S., Johnson, P.J., Chang, A.M., Hjelm, N.M., 1998. Am. J. Hum. Genet. 62, 768-775.

Luo, F., Lin, Y., Zheng, L., Lin, X., Chi, Y., 2015. ACS Appl. Mater. Inter. 7, 11322-11329.

Ma, M., Noei, H., Mienert, B., Niesel, J., Bill, E., Muhler, M., Fischer, R.A., Wang, Y., Schatzschneider, U., Metzler-Nolte, N., 2013. Chemistry. 19, 6785-6790.

Shiang, R., Thompson, L.M., Zhu, Y.Z., Church, D.M., Fielder, T.J., Bocian, M., Winokur, S.T., Wasmuth, J.J., 1994. Cell. 78, 335-342.

Shin, Y., Perera, A.P., Park, M.K., 2013. Sensor. Actuat. B-Ch. 178, 200-206.

Tabor, A., Alfirevic, Z., 2010. Fetal. Diagn. Ther. 27, 1-7.

Taylor-Pashow, K.M., Della Rocca, J., Xie, Z., Tran, S., Lin, W., 2009. J. Am. Chem. Soc. 131, 14261-14263.

Xie, S., Ye, J., Yuan, Y., Chai, Y., Yuan, R., 2015. Nanoscale. 7, 18232-18238.

Xu, Y., Li, X., Ge, H.J., Xiao, B., Zhang, Y.Y., Ying, X.M., Pan, X.Y., Wang, L., Xie, W.W., Ni, L., Chen, S.P., Jiang, W.T., Liu, P., Ye, H., Cao, Y., Zhang, J.M., Liu, Y., Yang, Z.J., Chen, Y.W., Chen, F., Jiang, H., Ji, X., 2015. Genet. Med. 17, 889-896.

Zhao, R., Ruan, Y., Wang, X., 2015. Int. J. Clin. Exp. Med. 8, 19241-19249.

Highlights

- We designed a non-invasive electrochemical DNA sensor for ultrasensitive detection of FGFR3 gene mutation.
- Hemin-MOFs/PtNPs composite was used for signal amplification.
- Biotin-Streptavidin system was utilized.